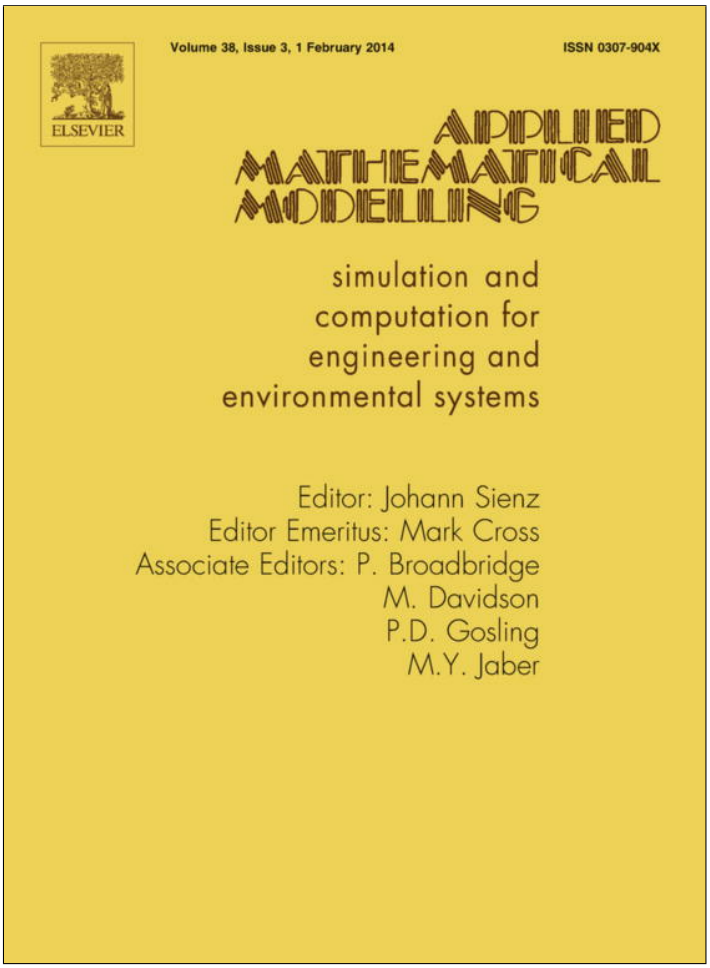

Applied Mathematical Modelling 38 (2014) 864–877

Contents lists available at ScienceDirect

Applied Mathematical Modelling

journal homepage: www.elsevier.com/locate/apm

Application of a heterogenous multiscale method to multi-batch driven pipeline

Sašo Blažič [a,*], Gerhard Geiger [b], Drago Matko [a]

[a] University of Ljubljana, Faculty of Electrical Engineering, Tržaška 25, SI-1000 Ljubljana, Slovenia
[b] Westfälische Hochschule Gelsenkirchen, Fachbereich Elektrotechnik und Angewandte Naturwissenschaften, Neidenburger Str. 43, 45897 Gelsenkirchen, Germany

ARTICLE INFO

Article history:
Received 10 January 2011
Received in revised form 2 June 2013
Accepted 2 July 2013
Available online 22 July 2013

Keywords:
Pipeline
Multiscale simulation
Lumped parameter model
Method of characteristics

ABSTRACT

The problem of simulating pipelines that are used for transporting different fluids is addressed in the paper. The model of the multi-batch pipeline is obtained by extending the classical "water hammer equations" (dealing with pressure and velocity of the medium) with fluid density. In such way a system of nonlinear partial differential equations is derived and solved by the method of characteristics. However, the ordinary differential equations resulting from the method of characteristics are defined on domains with very different slopes in the (x,t) space. A heterogenous multiscale method using two grids is capable of coping with associated numerical problems as shown by comparison of simulated and measured data on a real pipeline.

1. Introduction

Real time transient model (RTTM) based leak monitoring systems [1–3] require a sophisticated mathematical model of the flow in pipelines. The so called "water hammer equations" are relatively simple mathematical models assuming isentropic flow; they are obtained using the principles of mass and momentum conservation [4,5]. These models are based on a one-dimensional approach for one-phase liquid flow. Up to now, there is no analytical solution for this non-linear, partial differential equation system available. However, numerical techniques have traditionally been exploited to solve such problems. Several different approaches exist in the literature for tackling the aforementioned problem. Very often the method of characteristics [6] has been used, other approaches include finite volume [7], finite difference (explicit [8] or implicit [9,10]), finite element methods [11], polynomial differential quadrature [12], and transfer function modelling [13]. All these methods represent a part of the field of Computational Fluid Dynamics (CFD). The increased computational power of modern digital computer has steadily increased the range of possibilities in that field.

Not only RTTM based leak monitoring systems have been widely studied in the recent years, but also a handful of commercial products for RTTM based leak monitoring systems is offered. An excellent literature review of RTTM based leak detection methods can be found in [14]. It has been shown [15] that water-hammer wave attenuation, shape and timing parameters may be significantly affected by violating the idealised conditions of the water-hammer equations. Some approaches also dealt with turbulent flows [16,17] where vaned pipe bends are analysed in [17]. Yet, very little has been published on the simulation of multi-batch driven pipelines, where different fluids are transported through the same pipeline. A simple model of such pipelines was presented in [18].

* Corresponding author. Address: Tržaška 25, 1000 Ljubljana, Slovenia. Tel.: +386 1 4768763; fax: +386 1 4264631.
E-mail addresses: saso.blazic@fe.uni-lj.si (S. Blažič), gerhard.geiger@fh-gelsenkirchen.de (G. Geiger), drago.matko@fe.uni-lj.si (D. Matko).

0307-904X/$ - see front matter © 2013 Elsevier Inc. All rights reserved.
http://dx.doi.org/10.1016/j.apm.2013.07.001

The purpose of the present paper is to propose an alternative solution for simulation of multi-batch driven pipelines. This is achieved by extending the method of characteristic to multi-batch driven pipelines and by applying the heterogenous multi-scale method for the simulation of equations which are not defined on the same domain.

In Section 2 the simple water hammer equation model will be extended to the case when different fluids are transported through the same pipeline. This enables the description of multi-product flows with multiple products or batches being transported at the same time in one pipeline. The same model was used in [18], where the problem was linearised and solved analytically. In this paper, however, the method of characteristics [6] is applied to the extended model as shown in Section 3. The ordinary differential equations resulting from the method of characteristics are defined on domains with very different slopes in the (x,t) space. In order to circumvent this problem, a heterogenous multiscale method using two grids is proposed in Section 4. This method is capable of coping with associated numerical problems as shown in Section 5 presenting comparison of simulated and measured data on a real pipeline.

2. Mathematical model of the pipeline

The classical solution for unsteady flow problems is obtained by using the equations for continuity, momentum and energy. These equations correspond to the physical principles of mass, momentum and energy conservation. By applying these equations, a coupled non-linear set of partial differential equations is obtained that is very difficult to solve analytically. To date, there is no general closed-form solution. Further problems arise in the case of turbulent flow, which introduces stochastic flow behavior. Therefore, the mathematical derivation for the flow through a pipeline is a mixture of both theoretical and empirical approaches.

The following assumptions for the derivation of a mathematical model of the flow through pipelines are made:

1. *Fluid is compressible.* Compressibility of fluid results in an unsteady flow.
2. *Flow is viscous.* Viscosity causes shear stresses in a moving fluid.
3. *Flow is adiabatic.* No transfer of energy between fluid and pipeline will be considered.
4. *Flow is isothermal.* Temperature changes due to pressure changes can be neglected for liquids. Under these circumstances, temperature changes could only be result of friction effects, but these effects will also be neglected. Therefore, the temperature along the pipeline is supposed to be constant.
5. *Flow is one-dimensional.* All characteristics of the pipeline such as velocity v and pressure p depend only on the x-axis laid along the pipeline.

Consider now a pipeline of length L_p and with constant diameter

$$D = D(x) = 2R = const. \tag{1}$$

The continuity equation in conservative form for the one-dimensional case yields [11]

$$\frac{d\rho}{dt} + \rho\frac{\partial v}{\partial x} = 0, \tag{2}$$

with density $\rho(x,t)$, velocity $v(x,t)$, and with the substantial or total derivative

$$\frac{d\rho}{dt} \equiv \frac{\partial \rho}{\partial t} + v\frac{\partial \rho}{\partial x}. \tag{3}$$

The Momentum Equation in conservative form for the one-dimensional case yields [11]

$$\rho\frac{dv}{dt} = -\rho g\sin\alpha - \frac{\partial p}{\partial x} + \frac{\partial p_L}{\partial x}, \tag{4}$$

with pressure $p(x,t)$. The quantity $g\sin\alpha$ is the x-component of the standard gravity vector $\mathbf{g}$. The pressure loss p_L rely on the shear stress τ_R. The formula from Darcy and Weisbach [19] states that

$$\frac{\partial p_L}{\partial x} = -\rho\frac{\lambda v \mid v \mid}{2D}, \tag{5}$$

with the dimensionless friction coefficient $\lambda(v)$. This equation holds for the laminar flow as well as for the turbulent flow. Laminar flow is described by [19]

$$\lambda = \lambda(v) = \frac{64}{Re}, \tag{6}$$

if the dimensionless Reynolds number

$$Re = \frac{D}{v}\cdot v \tag{7}$$

is smaller than 2320 (v is the kinematic viscosity of the fluid). For larger values of the Reynolds number, flow is assumed to be turbulent. In that case, (6) can be replaced with an appropriately mixed theoretically and empirically derived formula such as the formula of Colebrook [19]

$$\frac{1}{\sqrt{\lambda}} = -2\log\left(\frac{2.51}{Re\sqrt{\lambda}} + 0.27\frac{k_R}{D}\right), \tag{8}$$

with roughness height k_R as a measure of the roughness of commercial pipes. Using Eqs. (4) and (5) we obtain

$$\frac{dv}{dt} + \frac{1}{\rho}\frac{\partial p}{\partial x} + g\sin\alpha + \frac{\lambda v \mid v \mid}{2D} = 0. \tag{9}$$

Using the definition of the (isentropic) speed of sound $a = \sqrt{dp/d\rho}$ the following equation is obtained

$$dp = a^2 d\rho. \tag{10}$$

The model of the pipeline is completed by modelling the invariance of fluid properties such as viscosity v and speed of sound a:

$$\frac{d\rho}{dt} + \rho\frac{\partial v}{\partial x} = 0, \tag{11}$$

$$\frac{dv}{dt} + \frac{1}{\rho}\frac{\partial p}{\partial x} + g\sin\alpha + \frac{\lambda v \mid v \mid}{2D} = 0, \tag{12}$$

$$\frac{dp}{dt} - a^2\frac{d\rho}{dt} = 0, \tag{13}$$

$$\frac{da}{dt} = 0, \tag{14}$$

$$\frac{dv}{dt} = 0. \tag{15}$$

The initial conditions for the above system are $p(x,0)$, $v(x,0)$, $\rho(x,0)$, $a(x,0)$, and $v(x,0)$. In order to solve the above system of partial differential equations, boundary conditions are also necessary. The first two boundary conditions concern the knowledge of pressure and/or velocity at the pipeline inlet/outlet. The pressure $p(0,t)$ or the velocity $v(0,t)$ has to be known at the pipeline inlet, while one of these two quantities also has to be known at the pipeline outlet. The possible combinations are therefore: $\{p(0,t), p(L_p,t)\}, \{p(0,t), v(L_p,t)\}, \{v(0,t), p(L_p,t)\}$, and $\{v(0,t), v(L_p,t)\}$. In this paper both pressures will be known. Furthermore, three boundary conditions for the density, the speed of sound, and the viscosity are needed. Namely, $\rho(0,t), a(0,t)$, and $v(0,t)$ will be used as boundary conditions if $v(0,t) \geqslant 0$. If, on the other hand, $v(0,t) < 0$, the following boundary conditions will be known: $\rho(L_p,t), a(L_p,t)$, and $v(L_p,t)$.

3. Method of characteristics

First, the system of PDEs, represented by Eqs. (11)–(15), will be transformed into the form that is more suitable for the consequent operations. Note that Eqs. (14) and (15) are independent from Eqs. (11)–(13) in the sense that their solutions do not depend on solutions of the other three equations. The first three equations are rewritten again by replacing the total derivatives with the partial ones ($\frac{d\rho}{dt} = \frac{\partial\rho}{\partial t} + v\frac{\partial\rho}{\partial x}$, $\frac{dv}{dt} = \frac{\partial v}{\partial t} + v\frac{\partial v}{\partial x}$, $\frac{dp}{dt} = \frac{\partial p}{\partial t} + v\frac{\partial p}{\partial x}$), by defining a state vector

$$\mathbf{y} = \begin{bmatrix} \rho \\ v \\ p \end{bmatrix}, \tag{16}$$

matrices

$$\mathbf{A}_t = \begin{bmatrix} 1 & 0 & 0 \\ 0 & 1 & 0 \\ -a^2 & 0 & 1 \end{bmatrix}, \tag{17}$$

$$\mathbf{A}_x = \begin{bmatrix} v & \rho & 0 \\ 0 & v & 1/\rho \\ -a^2 v & 0 & v \end{bmatrix} \tag{18}$$

and a vector

$$\mathbf{b} = \begin{bmatrix} 0 \\ g\sin\alpha + \frac{\lambda v|v|}{2D} \\ 0 \end{bmatrix}, \tag{19}$$

to come up with the following vector partial differential equation:

$$\mathbf{A}_t \frac{\partial \mathbf{y}}{\partial t} + \mathbf{A}_x \frac{\partial \mathbf{y}}{\partial x} + \mathbf{b} = 0. \tag{20}$$

Using the eigenvector transformation of $\mathbf{A}_t^{-1}\mathbf{A}_x$

$$\mathbf{A}_t^{-1}\mathbf{A}_x = \begin{bmatrix} v & \rho & 0 \\ 0 & v & 1/\rho \\ 0 & a^2\rho & v \end{bmatrix} = \mathbf{\Theta}\mathbf{\Lambda}\mathbf{\Theta}^{-1}, \tag{21}$$

where

$$\mathbf{\Theta} = \begin{bmatrix} \frac{1}{2a^2} & \frac{1}{2a^2} & -\frac{1}{a^2} \\ \frac{1}{2a\rho} & -\frac{1}{2a\rho} & 0 \\ \frac{1}{2} & \frac{1}{2} & 0 \end{bmatrix} \tag{22}$$

is the matrix of the eigenvectors of $\mathbf{A}_t^{-1}\mathbf{A}_x$ and

$$\mathbf{\Lambda} = \begin{bmatrix} v+a & 0 & 0 \\ 0 & v-a & 0 \\ 0 & 0 & v \end{bmatrix} \tag{23}$$

is the diagonal matrix of the corresponding eigenvalues, the following equation is obtained

$$\mathbf{\Theta}^{-1}\frac{\partial \mathbf{y}}{\partial t} + \mathbf{\Lambda}\mathbf{\Theta}^{-1}\frac{\partial \mathbf{y}}{\partial x} + \mathbf{\Theta}^{-1}\mathbf{A}_t^{-1}\mathbf{b} = 0, \tag{24}$$

where

$$\mathbf{\Theta}^{-1} = \begin{bmatrix} 0 & a\rho & 1 \\ 0 & -a\rho & 1 \\ -a^2 & 0 & 1 \end{bmatrix}, \tag{25}$$

$$\mathbf{\Lambda}\mathbf{\Theta}^{-1} = \begin{bmatrix} 0 & (v+a)a\rho & v+a \\ 0 & -(v-a)a\rho & v-a \\ -va^2 & 0 & v \end{bmatrix}, \tag{26}$$

$$\mathbf{\Theta}^{-1}\mathbf{A}_t^{-1}\mathbf{b} = \begin{bmatrix} a\rho\left(g\sin\alpha + \frac{\lambda v|v|}{2D}\right) \\ -a\rho\left(g\sin\alpha + \frac{\lambda v|v|}{2D}\right) \\ 0 \end{bmatrix}. \tag{27}$$

The vector partial differential Eq. (24) can be rewritten again as a set of scalar partial differential equations:

$$\left[\frac{\partial p}{\partial t} + (v+a)\frac{\partial p}{\partial x}\right] + a\rho\left[\frac{\partial v}{\partial t} + (v+a)\frac{\partial v}{\partial x}\right] + a\rho\left(g\sin\alpha + \frac{\lambda v \mid v \mid}{2D}\right) = 0, \tag{28}$$

$$\left[\frac{\partial p}{\partial t} + (v-a)\frac{\partial p}{\partial x}\right] - a\rho\left[\frac{\partial v}{\partial t} + (v-a)\frac{\partial v}{\partial x}\right] - a\rho\left(g\sin\alpha + \frac{\lambda v \mid v \mid}{2D}\right) = 0, \tag{29}$$

$$\left[\frac{\partial p}{\partial t} + v\frac{\partial p}{\partial x}\right] - a^2\left[\frac{\partial \rho}{\partial t} + v\frac{\partial \rho}{\partial x}\right] = 0, \tag{30}$$

The above set of PDEs is valid on the entire (x,t) space. The solution is quite difficult. The idea of method of characteristics is that the PDEs are not solved everywhere. Rather, some lines, called characteristics, are defined, and the PDEs are solved only on these lines. Thus the system of PDEs is transformed into the system of ordinary differential equations (ODE). Three characteristics are defined for our purposes:

- $\frac{dx}{dt} = v + a$, denoted by C^+,
- $\frac{dx}{dt} = v - a$, denoted by C^-, and
- $\frac{dx}{dt} = v$, denoted by C^F.

By introducing the above equations in Eqs. (28)–(30), the expressions in the square brackets become total derivatives if the proper characteristics are taken into account. The substitution yields the following:

$$dp + a\rho dv + a\rho\left(g\sin\alpha + \frac{\lambda v \mid v \mid}{2D}\right)dt = 0 \ (\text{valid on} C^{+}), \tag{31}$$

$$dp - a\rho dv - a\rho\left(g\sin\alpha + \frac{\lambda v \mid v \mid}{2D}\right)dt = 0 \ (\text{valid on} C^{-}), \tag{32}$$

$$dp - a^2 d\rho = 0 \ \left(\text{valid on} C^{F}\right). \tag{33}$$

Eqs. (14) and (15) can be rewritten as:

$$\frac{da}{dt} = \frac{\partial a}{\partial t} + v\frac{\partial a}{\partial x} = 0, \tag{34}$$

$$\frac{dv}{dt} = \frac{\partial v}{\partial t} + v\frac{\partial v}{\partial x} = 0, \tag{35}$$

Since $\frac{dx}{dt} = v$ defines characteristic C^F, these two equations are valid only on C^F. The system given by Eqs. (31)–(33) is completed by the following two equations:

$$da = 0 \ (\text{valid on} C^{F}), \tag{36}$$

$$dv = 0 \ (\text{valid on} C^{F}). \tag{37}$$

4. The heterogenous multiscale method

The method of characteristics yields five ordinary differential Eqs. 31, 32, 33, 36, 37 for five variables (p, v, ρ, a, v). The problem is that they are not defined on the same domain. Rather, the definition domains of the equations are different. They are given by the characteristics C^+, C^-, and C^F as illustrated in Fig. 1. The only way to solve this system of equations is to solve it numerically. However due to $v \ll a$ the slopes $(\frac{dt}{dx})$ of characteristics C^+ and C^- ($\frac{1}{v+a}$ and $\frac{1}{v-a}$, respectively) are much smaller than the slope of characteristic C^F $(\frac{1}{v})$. In order to avoid numerical problems two grids are needed.

First we need to choose the temporal resolution Δt which is done based on the system dynamics as in any simulation. Usually the resolution is selected in the range of a second. The spatial resolution is defined by the characteristics: the steep characteristics C^F (the slope is $\frac{1}{v}$) define micro-grid points whereas the characteristics with gradual slope C^+ and C^- (the slope is $\frac{1}{v\pm a}$) define the macro-grid points. But one also needs to have the stability of the algorithm in mind when choosing the spatial resolution. A necessary condition for the convergence of the studied partial differential equations numerically by the method of finite differences is the so-called Courant–Friedrichs–Lewy condition [20,21] which states that the mathematical domain of dependence should be contained in the numerical domain of dependence for each pair (x, t). When solving the fast dynamics given by Eqs. (31) and (32), the mathematical domain of dependence is the triangle RSP while the numerical domain of dependence is the triangle given by the points $(i-1, k), (i+1, k)$, and $(i, k+1)$ in Fig. 1. When solving the slow dynamics given by Eqs. (33), (36), and (37), the mathematical domain of dependence is the triangle TOP while the numerical domain of dependence is the triangle given by the points $(j-1, k), (j+1, k)$, and $(j, k+1)$ in Fig. 1. Consequently, in order to

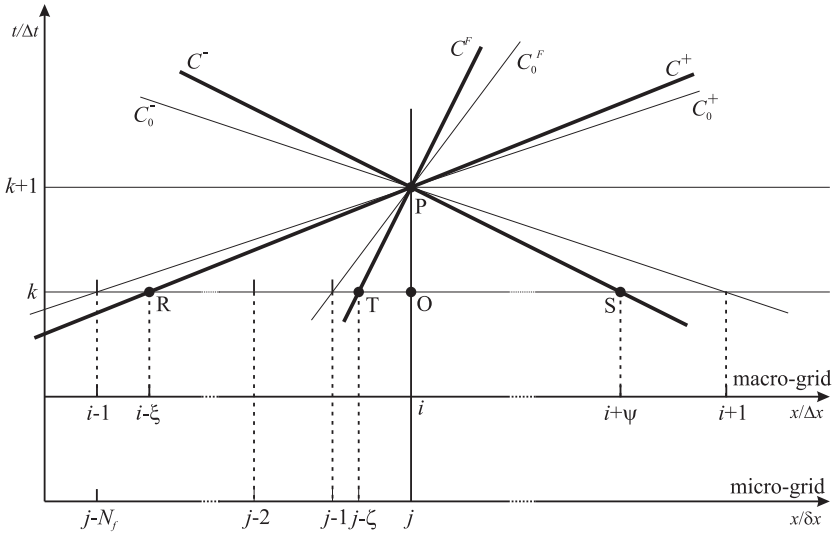

Fig. 1. The characteristics.

meet the necessary condition for the convergence of numerical results, the characteristics with the most gradual possible slope are defined. These characteristics are denoted by C_0^F, C_0^+, and C_0^- and are also shown in Fig. 1. These characteristics actually exactly define the points on both grids. This means that the temporal resolution of the micro-grid δx is defined by the equation:

$$\frac{\Delta t}{\delta x} \leqslant \min \frac{1}{|v|} = \frac{1}{\max |v|} \;\Rightarrow\; \delta x \geqslant \Delta t \max |v|, \tag{38}$$

which means that the spatial resolution of the micro-grid points is defined by the maximal expected velocity of the fluid. Note that the absolute value is used to also include the possibility of the pipeline running in reverse. Similarly, the macro-grid spatial resolution Δx is defined by the slope of C_0^+ and C_0^- (the absolute value of their slope is the same):

$$\frac{\Delta t}{\Delta x} \leqslant \frac{1}{\max |v| + \max a} \;\Rightarrow\; \Delta x \geqslant \Delta t(\max |v| + \max a), \tag{39}$$

which means that the spatial resolution of the macro-grid points is defined by the maximal expected velocity of the fluid and the largest possible sound speed of a medium in multi–batch operation. In order to simplify the numerical calculations, actual values of both spatial resolutions are obtained by first dividing the length of the pipeline L_p by an appropriate integer (denoted by N_r) to get the macro-grid resolution Δx, and then dividing the latter by an appropriate integer (denoted by N_f) to get the micro-grid resolution δx. In a practical implementation of the algorithm these two integers need to be chosen in accordance with the following inequalities based on Eqs. (38) and (39):

$$N_r = \frac{L_p}{\Delta x} \leqslant \frac{L_p}{\Delta t(\max |v| + \max a)}, \tag{40}$$

$$N_f = \frac{\Delta x}{\delta x} = \frac{L_p}{N_r \delta x} \leqslant \frac{L_p}{N_r \Delta t \max |v|}. \tag{41}$$

The characteristic C^+ has the slope $\frac{1}{v+a}$ and intersects the line $t = k\Delta t$ at the point R located at $x = (i - \xi)\Delta x$ where $\xi = (a + v)\frac{\Delta t}{\Delta x}$. The characteristic C^- has the slope $\frac{1}{v-a}$ and intersects the line $t = k\Delta t$ at the point S located at $x = (i + \psi)\Delta x$ where $\psi = (a - v)\frac{\Delta t}{\Delta x}$. The characteristic C^F intersects the line $t = k\Delta t$ at the point T located at $x = (j - \zeta)\delta x$ where $\zeta = v\frac{\Delta t}{\delta x} = N_f v \frac{\Delta t}{\Delta x}$. Due to the inequalities (38) and (39), the resulting ξ, ψ, and ζ always belong to the interval $[0, 1]$.

The two grids for the spatial variable x characterize a stiff system. So the proposed solution resembles the multiscale methods for stiff ordinary differential equations [22]. The variables p and v are calculated on the macro-grid, while ρ, a, and v on the micro-grid, respectively. Eqs. (31), (32), (33), (36) and (37) can be rewritten in the integral form

$$\int_R^P dp + \int_R^P a\rho dv + \int_R^P a\rho\left(g\sin\alpha + \frac{\lambda v\,|\,v\,|}{2D}\right)dt = 0, \tag{42}$$

$$\int_S^P dp - \int_S^P a\rho dv - \int_S^P a\rho\left(g\sin\alpha + \frac{\lambda v\,|\,v\,|}{2D}\right)dt = 0, \tag{43}$$

$$\int_T^P dp - \int_T^P a^2 d\rho = 0, \tag{44}$$

$$\int_T^P da = 0, \tag{45}$$

$$\int_T^P dv = 0. \tag{46}$$

The basic algorithm for the simulation of multi-batch driven pipelines is given next:

0. Initialise the simulation time ($k = 0$). Initialise all the macro-grid and the micro-grid variables from the initial condition of the system. Linear interpolation is used where necessary.
1. Make a simple prediction of micro-grid variables on the time interval $[k\Delta t,\ (k+1)\Delta t]$ based on the state in the time instant $t = k\Delta t$.
2. Determine the slope of the characteristics and the coefficients of the macro-grid equations by averaging the micro-grid variables.
3. Use the averaged values to solve the macro-grid system on the time interval $[k\Delta t,\ (k+1)\Delta t]$.
4. Having actual values of the macro-grid system solution, solve the micro-grid system again.
5. Unless the finish time is reached, increment k and go to step 1.

To simplify the notation, $\Delta x, \delta x$, and Δt will be omitted in the description of the variables, e.g., $v(j, k)$ will be used instead of $v(j\delta x, k\Delta t)$. Furthermore, V and P will be introduced to denote velocities and pressures on the macro-grid. The connection between the micro-grid and the macro-grid variables is straight-forward:

$$V(i,k) = v(iN_f,k), \tag{47}$$
$$P(i,k) = p(iN_f,k). \tag{48}$$

Next, the steps of the above algorithm will be discussed in detail.

4.1. Step 1

Micro-grid variables ρ, a and v are defined by Eqs. (44)–(46) are valid on the C^F characteristic. The slope of this characteristic is determined by the actual velocity of the fluid. According to the proposed algorithm, the initial fluid velocity $v(j,k)$ is used to determine the slope of the characteristic C^F connecting points T (located at $(j-\zeta,k)$) and P (located at $(j,k+1)$). The solutions of Eqs. (45) and (46) are

$$a(j,k+1) - a(j-\zeta,k) = 0, \tag{49}$$
$$v(j,k+1) - v(j-\zeta,k) = 0, \tag{50}$$

which means that the fluid properties v and a propagate along C^F characteristic unchanged. Linear interpolation is used for approximating the variables between the micro-grid points. Only the interpolation for $a(j-\zeta,k)$ is given here (the other variables are interpolated similarly):

$$a(j-\zeta,k) = \zeta a(j-1,k) + (1-\zeta)a(j,k). \tag{51}$$

Please note that the speed of sound a remains constant along the C^F characteristic. Since the speed of sound is quite large, the density change on the considered section of the C^F characteristic of Eq. (44) is very small and the initial estimate of the density ρ at the point P is

$$\hat{\rho}(j,k+1) = \rho(j-\zeta,k) \tag{52}$$

and so is on the entire section $\overline{TP}$ of the C^F characteristic. In step 4 this initial prediction of the density will be corrected taking into account calculated value of pressure in Eq. (44). The dimensionless friction coefficient λ on this section is calculated using the fluid velocity $v(j-\zeta,k)$ which is obtained by the linear interpolation.

4.2. Step 2

The slope of the characteristics C^+ and C^- is obtained by averaging the speed of sound and the fluid velocity on the sections $[i-1,i]$ and $[i,i+1]$, respectively:

$$\bar{a}|_{i-1}^{i} = \frac{1}{N_f}\sum_{\mathcal{L}=0}^{N_f-1} a(j-\mathcal{L},k)\,\bar{v}|_{i-1}^{i} = \frac{1}{N_f}\sum_{\mathcal{L}=0}^{N_f-1} v(j-\mathcal{L},k), \tag{53}$$
$$\bar{a}|_{i}^{i+1} = \frac{1}{N_f}\sum_{\mathcal{L}=0}^{N_f-1} a(j+\mathcal{L},k)\,\bar{v}|_{i}^{i+1} = \frac{1}{N_f}\sum_{\mathcal{L}=0}^{N_f-1} v(j+\mathcal{L},k). \tag{54}$$

Using the slopes obtained by average velocities the characteristics C^+ and C^- (i.e. points R and S) can be determined and the coefficients of the macro-grid equations, valid on these characteristics, are obtained by averaging the micro-grid variables a, λ, and ρ. The averaged coefficients are

$$\bar{\varphi}_{RP} = \overline{a\rho}|_R^P, \tag{55}$$
$$\bar{\varphi}_{SP} = \overline{a\rho}|_S^P, \tag{56}$$
$$\bar{\varphi}_{RP}^{\alpha} = \overline{a\rho g\sin(\alpha)}|_R^P, \tag{57}$$
$$\bar{\varphi}_{SP}^{\alpha} = \overline{a\rho g\sin(\alpha)}|_S^P, \tag{58}$$
$$\bar{\varphi}_{RP}^{\lambda} = \frac{1}{2D}\overline{a\rho\lambda}|_R^P, \tag{59}$$
$$\bar{\varphi}_{SP}^{\lambda} = \frac{1}{2D}\overline{a\rho\lambda}|_S^P. \tag{60}$$

Since the best predictions of a, ρ and λ remain constant on the C^F characteristic, the average on sections RP and SP can be replaced by the average on sections RT and TS, respectively.

4.3. Step 3

Using the averaged coefficients, the macro-grid Eqs. (42) and (43) can be integrated. Several methods will be studied here. They are given in the following.

4.3.1. Euler method

Euler method is a simple explicit integration method where the function values on the integration interval are replaced by their initial values. In our case this applies to the term $v|v|$ in Eqs. (42) and (43) yielding

$$(P(i,k+1)-P(i-\xi,k))+\bar{\varphi}_{RP}(V(i,k+1)-V(i-\xi,k))+\bar{\varphi}^{\alpha}_{RP}+\bar{\varphi}^{\lambda}_{RP}V(i-\xi,k)\mid V(i-\xi,k)\mid \Delta t=0, \tag{61}$$

$$(P(i,k+1)-P(i+\psi,k))-\bar{\varphi}_{SP}(V(i,k+1)-V(i+\psi,k))-\bar{\varphi}^{\alpha}_{SP}-\bar{\varphi}^{\lambda}_{SP}V(i+\psi,k)\mid V(i+\psi,k)\mid \Delta t=0, \tag{62}$$

where $P(i-\xi,k), V(i-\xi,k), P(i+\psi,k)$, and $V(i+\psi,k)$ are obtained by linear interpolation similarly as in Eq. (51).

Eqs. (61) and (62) represent a system of two equations with two unknowns ($P(i,k+1)$ and $V(i,k+1)$) which can be solved analytically yielding

$$\begin{aligned}P(i,k+1)=&\frac{1}{\bar{\varphi}_{RP}+\bar{\varphi}_{SP}}(\bar{\varphi}_{SP}P(i-\xi,k)+\bar{\varphi}_{RP}P(i+\psi,k)-\bar{\varphi}_{RP}\bar{\varphi}_{SP}V(i+\psi,k)+\bar{\varphi}_{RP}\bar{\varphi}_{SP}V(i-\xi,k)\\&+(\bar{\varphi}_{RP}\bar{\varphi}^{\alpha}_{SP}-\bar{\varphi}_{SP}\bar{\varphi}^{\alpha}_{RP})\Delta t+\bar{\varphi}_{RP}\bar{\varphi}^{\lambda}_{SP}V(i+\psi,k)\mid V(i+\psi,k)\mid \Delta t-\bar{\varphi}_{SP}\bar{\varphi}^{\lambda}_{RP}V(i-\xi,k)\mid V(i-\xi,k)\mid \Delta t)\end{aligned} \tag{63}$$

$$\begin{aligned}V(i,k+1)=&\frac{1}{\bar{\varphi}_{RP}+\bar{\varphi}_{SP}}(P(i-\xi,k)-P(i+\psi,k)-+\bar{\varphi}_{RP}V(i-\xi,k)+\bar{\varphi}_{SP}V(i+\psi,k)-(\bar{\varphi}^{\alpha}_{RP}+\bar{\varphi}^{\alpha}_{SP})\Delta t\\&-\bar{\varphi}^{\lambda}_{RP}V(i-\xi,k)\mid V(i-\xi,k)\mid \Delta t-\bar{\varphi}^{\lambda}_{SP}V(i+\psi,k)\mid V(i+\psi,k)\mid \Delta t\end{aligned} \tag{64}$$

The solutions for the inlet and the outlet points are a bit different – the boundary conditions must be taken into consideration. For the inlet point only the C^- characteristic (Eq. 62) is used for $i=0$ yielding

$$V(0,k+1)=\frac{P(0,k+1)}{\bar{\varphi}_{SP_0}}-\frac{P(0+\psi,k)}{\bar{\varphi}_{SP_0}}+V(0+\psi,k)-g\sin(\alpha_0)\Delta t-\bar{\lambda}_{SP_0}V(0+\psi,k)\mid V(0+\psi,k)\mid \Delta t, \tag{65}$$

where

$$\lambda_{SP_0}=\frac{1}{2D}\bar{\lambda}|^{P_0}_{S}. \tag{66}$$

P_0 is the point at the inlet at the moment $t=(k+1)\Delta t$ and α_0 is the inclination of the pipeline at the inlet.

For the outlet point only the C^+ characteristic (Eq. 61) is used yielding

$$V(N_r,k+1)=\frac{P(N_r-\xi,k)}{\bar{\varphi}_{RP_N}}-\frac{P(N_r,k+1)}{\bar{\varphi}_{RP_N}}+V(N_r-\xi,k)-g\sin(\alpha_N)\Delta t-\bar{\lambda}_{RP_N}V(N_r-\xi,k)\mid V(N_r-\xi,k)\mid \Delta t, \tag{67}$$

where

$$\lambda_{RP_N}=\frac{1}{2D}\bar{\lambda}|^{P_N}_{R} \tag{68}$$

and P_N is the point at the outlet at the moment $t=(k+1)\Delta t$ while α_N is the inclination of the pipeline at the outlet.

4.3.2. Trapezoidal method

Using the trapezoidal method the term $v\mid v\mid$ is replaced by $(V(i-\xi,k)\mid V(i-\xi,k)\mid +V(i,k+1)\mid V(i,k+1)\mid)/2$ and $(V(i+\psi,k)\mid V(i+\psi,k)\mid +V(i,k+1)\mid V(i,k+1)\mid)/2$ for the C^+ and the C^- characteristic, respectively. Two nonlinear equations are obtained and since they have no analytical solutions, an iteration should be used. However if the term $v|v|$ is replaced by $\mathrm{sign}(V(i,k))V^2$ a system of two quadratic equations is obtained, which can be solved analytically and has two solutions. However only for one of them $V(i,k+1)$ has the same sign as $V(i,k)$ and this solution shall be used. The solutions are given in Appendix A.

4.3.3. Approximative trapezoidal method

We denote fluid velocities in points R, P and S by V_R, V_P and V_S respectively. With this method the term $v|v|$ is first replaced by $\mathrm{sign}(V_R)V^2$. Applying the trapezoidal method V^2 is replaced by $(V_R^2+V_P^2)/2$ for the C^+ characteristic. Then V_P is replaced by $V_R+\Delta V$ and the quadratic term $(\Delta V)^2$ is neglected. This results finally in

$$v|v|\approx \mathrm{sign}(V_R)V^2=\mathrm{sign}(V_R)\left(V_R^2+(V_R+\Delta V)^2\right)/2\approx \mathrm{sign}(V_R)(V_R^2+V_RV_P)=|V_R|V_P. \tag{69}$$

Similarly for the C^- characteristic the term $v|v|$ is replaced by $|V_S|V_P$. In such way a system of two linear equations is obtained and the solutions are given in Appendix B.

4.4. Step 4

In the previous step, pressures and velocities were obtained on the macro-grid and will be now interpolated to obtain their values on the micro-grid:

$$p(j,k) = \left(1 - \frac{j - iN_f}{N_f}\right) P(i,k) + \frac{j - iN_f}{N_f} P(i+1,k),\ iN_f \leqslant j < (i+1)N_f, \tag{70}$$

$$v(j,k) = \left(1 - \frac{j - iN_f}{N_f}\right) V(i,k) + \frac{j - iN_f}{N_f} V(i+1,k),\ iN_f \leqslant j < (i+1)N_f. \tag{71}$$

Having the values of the pressure on the micro-grid, the density along the micro-grid can be calculated again (the rough prediction of the density was calculated in step 1, Eq. (52)) from Eq. (44):

$$\rho(j,k+1) = \rho(j-\zeta,k) + \frac{p(j,k+1) - p(j-\zeta,k)}{a^2(j-\zeta,k)}. \tag{72}$$

4.5. Stability of the algorithm vs. numerical diffusion

As already said, the stability aspect is extremely important when choosing an appropriate spatial resolution. The spatial resolutions of both grids, Δx and δx, respectively, should be chosen large enough (Eqs. 38 and 39) to meet the requirement of the Courant–Friedrichs–Lewy condition. As a consequence, variables ξ, ψ, and ζ never exceed 1. In order to calculate the variables at $t = (k+1)\Delta t$, the values at $t = k\Delta t$ on the corresponding characteristics are needed. The latter are obtained by means of interpolation which induces numerical diffusion. The numerical diffusion is less obvious when the variables ξ, ψ, and ζ are closer to 0 or to 1.

In multi-batch operation with fluids having different speeds of sound the macro-grid points for calculating pressures and velocities are chosen in accordance with the highest speed of sound. If the speed of sound of a particular fluid is around a half of the maximal speed of sound, the numerical-diffusion effect is strongest. Similarly, on the micro-grid the numerical diffusion is strongest if the current velocity of the fluid is around a half of the maximal expected fluid velocity. This influences the simulated values of density, viscosity and speed of sound along the pipeline.

In conclusion, the diffusion effect is strongest when the algorithm is far from the stability boundary. When the velocity increases, the numerical diffusion is lower, but the algorithm approaches instability boundary.

5. Validation of the model

The proposed model was validated on a real pipeline with the following data: length of the pipeline $L_p = 9854$ m, diameter $D = 0.2065$ m, roughness $k_R = 0.118$ mm, and inclination $\alpha = -0.00256$ rad. The dynamical properties of the model can be analysed during batch changes, so the data were recorded in an operation phase where the batch changed twice. The speeds of sound a for the three batches were 1113.5, 985.4, and 916.6 m/s, while the kinematic viscosities v were 0.72, 0.52, and 0.70 mm^2/s, respectively.

In order to simulate the pipeline, the initial and the boundary conditions are also needed as already discussed in Section 2. Due to operational reasons the pipeline must be stopped before and after a batch change. At the beginning of the experiment, the pipeline was was not running. It was full of the first batch. The pressures were measured at the inlet and and the outlet of the pipeline constantly. The initial measurements were $p(0,0) = 2.4648 \cdot 10^6$ N/m^2 and $p(L_p,0) = 2.6715 \cdot 10^6$ N/m^2. The linear profile of the initial pressure is assumed, so the initial conditions for the simulation are:

- $p(x,0) = p(L_p,0)\frac{x}{L_p} + p(0,0)(1 - \frac{x}{L_p})$,
- $v(x,0) = 0$ m/s,
- $\rho(x,0) = 831.42$ kg/m^3,
- $a(x,0) = 1113.5$ m/s, and
- $v(x,0) = 0.72$ mm^2/s.

Note that the arguments of all the functions in this section are x and t (and not i, j, and k).

The following boundary conditions will be used in the simulation:

- the measured pressure at the pipeline inlet $p(0,t)$ (shown in Fig. 2 with the blue line),
- the measured pressure at the pipeline outlet $p(L_p,t)$ (shown in Fig. 2 with the red line),
- the measured density at the pipeline inlet $\rho(0,t)$ (shown in Fig. 3 with the dashed line),
- speed of sound at the pipeline inlet $a(0,t)$ (defined with batch changes), and
- kinematic viscosity at the pipeline inlet $v(0,t)$ (defined with batch changes).

The outputs of the simulation model are:

- the fluid speed at the pipeline inlet $v(0,t)$,
- the fluid speed at the pipeline outlet $v(L_p,t)$, and
- the fluid density at the pipeline outlet $\rho(L_p,t)$.

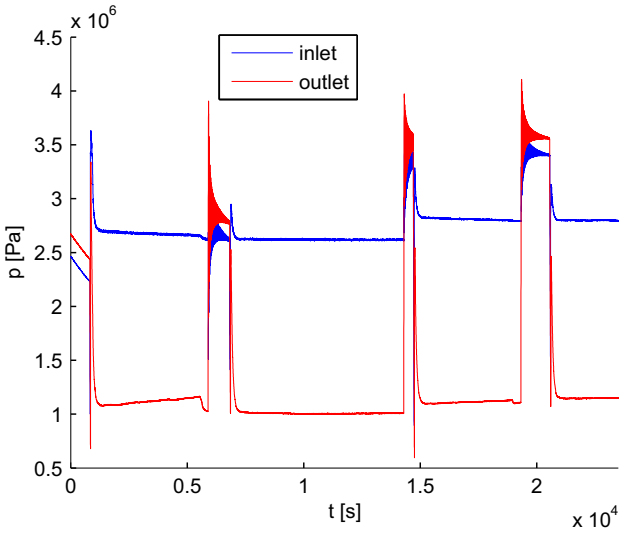

Fig. 2. The time course of the pressures at the inlet and the outlet of the pipeline.

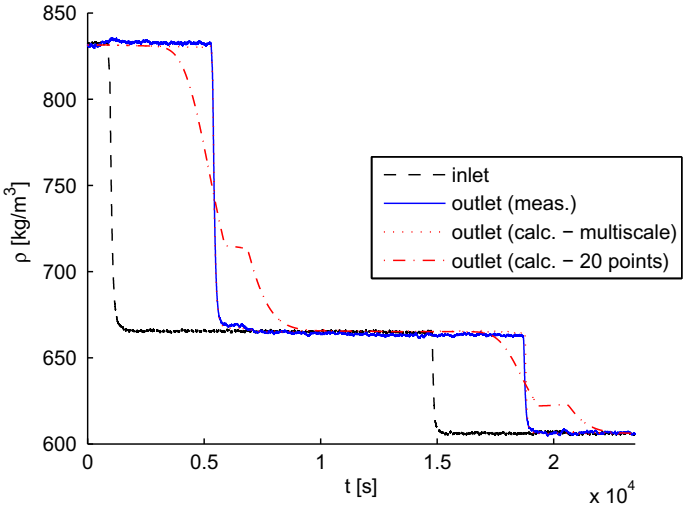

Fig. 3. The time course of the density ρ at the inlet (black dashed line) and the outlet of the pipeline (measured – blue solid line; one-scale-model response – red dash-dotted line; multiscale-model response – red dotted line). (For interpretation of the references to colour in this figure caption, the reader is referred to the web version of this article.)

All these three variables were also measured during the operation and now these measurements will be compared to the simulation outputs.

In the simulation of the proposed multiscale method, the temporal resolution is chosen as $\Delta t = 0.44$ s, the number of macro-grid intervals was chosen to be $N_r = 20$ (taking into account maximal speed of sound 1113.5 m/s and maximal expected velocity of the fluid 2.8 m/s) while the number of micro-grid intervals inside a macro-grid interval was $N_f = 400$ (taking into account maximal expected velocity of the fluid 2.8 m/s). These settings guarantee stable simulation in the studied case. All three proposed integration methods (Euler, trapezoidal, trapezoidal approximative) were used for simulation and the results were practically the same (the differences between the responses of the three models were far below the measurement noise). Consequently, the figures of responses show only one variable when referring to the multiscale method. The proposed heterogenous multiscale method was compared to the classical one-scale method. Two settings for the one-scale method were used: 20 intermediate intervals or points and 500 intermediate intervals or points. Fig. 3 shows the time plots of the densities at the outlet of the pipeline. The measured output is depicted with the solid line, the multiscale-model response with the dotted line, and the one-scale-model response with the dash-dotted line. The batch changes (1000 s to 5300 s and 14800 s to 19000 s) can be clearly seen. The integral square error criteria for the three models are shown in Table 1. The table also also gives computational complexity of the algorithms in terms of the time needed to calculate model response. The algorithms were implemented in Matlab and run on an Intel Xeon CPU 2.8 GHz computer with 1 GB of RAM. Note that calculation time of the proposed method is much shorter than in the case of the one-scale method with 500 points. In the former case the complex equations for the velocity and the pressure (e.g. Eqs. (63) in (64)) are only

Table 1
The comparison of the three algorithms for the simulation of the pipeline (e is the modelling error – the difference between the measured and the simulated density at the pipeline outlet, T_{fin} is the simulation time).

	one-scale method (20 points)	one-scale method (500 points)	multiscale method (20x400 points)
$\int_0^{T_{fin}} e^2(\tau)d\tau$ [kg^{2}s/m^6]	$8.08 \cdot 10^6$	$5.89 \cdot 10^5$	$1.29 \cdot 10^5$
Calculation time	10 min	69 h	48 min

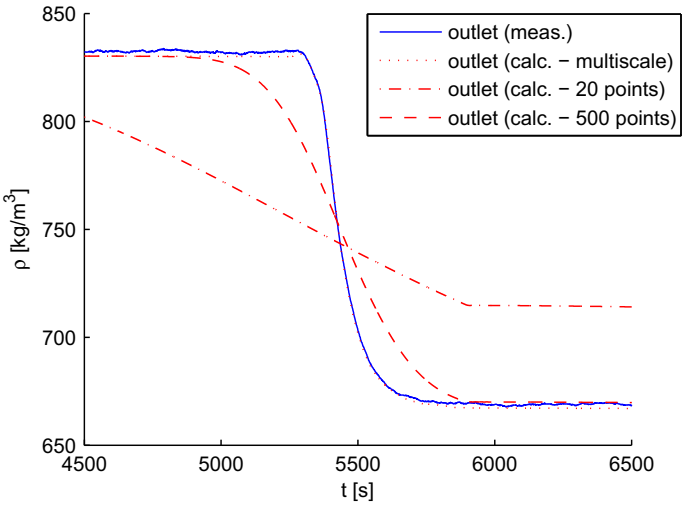

Fig. 4. A detail of the outlet density time plot (measured – blue solid line; one-scale-model response with 20 points – red dash-dotted line; one-scale-model response with 500 points – red dashed line; multiscale-model response – red dotted line). (For interpretation of the references to colour in this figure caption, the reader is referred to the web version of this article.)

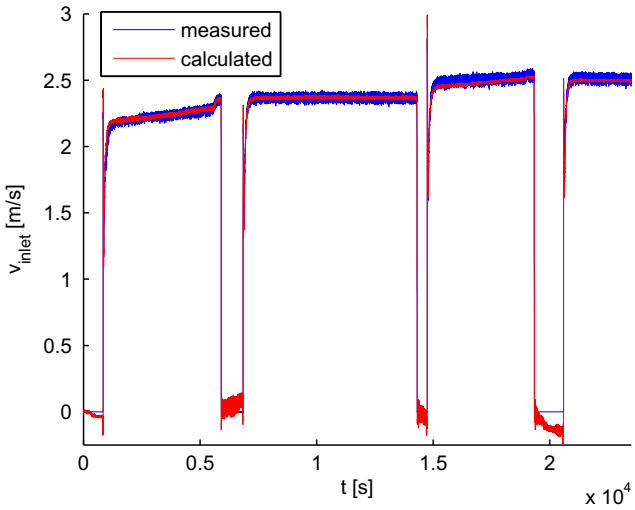

Fig. 5. The time plots of the fluid velocities at the inlet of the pipeline: measured (blue), multiscale-model response (red).

calculated 20 times, while the simple equations for the other three variables are performed 8000 times. In the latter case the complete model has to be evaluated 500 times. Thus a huge difference between the calculation time is explained. While the model response of the proposed multiscale simulation method corresponds very well to the measured data (see Table 1), the results of the classical one-scale method with 20 points exhibit smoothing of the batch flanks due to numerical diffusion. The numerical diffusion is so high that the pipeline is stopped before the simulated batch flank has reached the outlet of the pipeline, causing a step in the time course of the simulated density ρ. Even if the number of inner points is increased significantly (from 20 to 500, which increases the computational load dramatically – from 10 min to 69 h), the numerical diffusion can not be eliminated as can be seen in Fig. 4 depicting a detail of the batch transient phase.

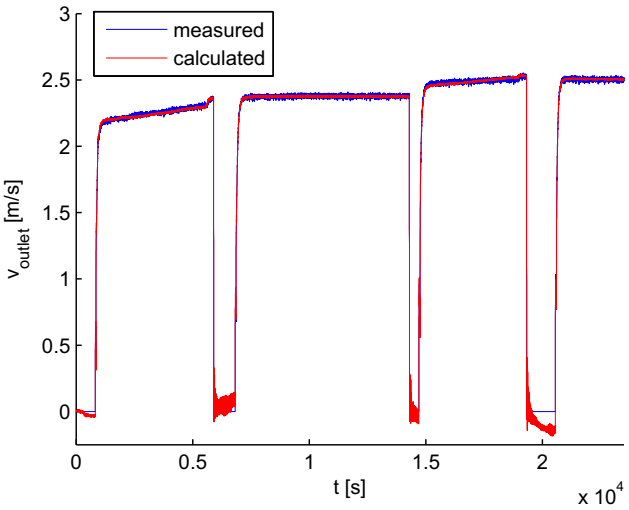

Fig. 6. The time plots of the fluid velocities at the outlet of the pipeline: measured (blue), multiscale-model response (red).

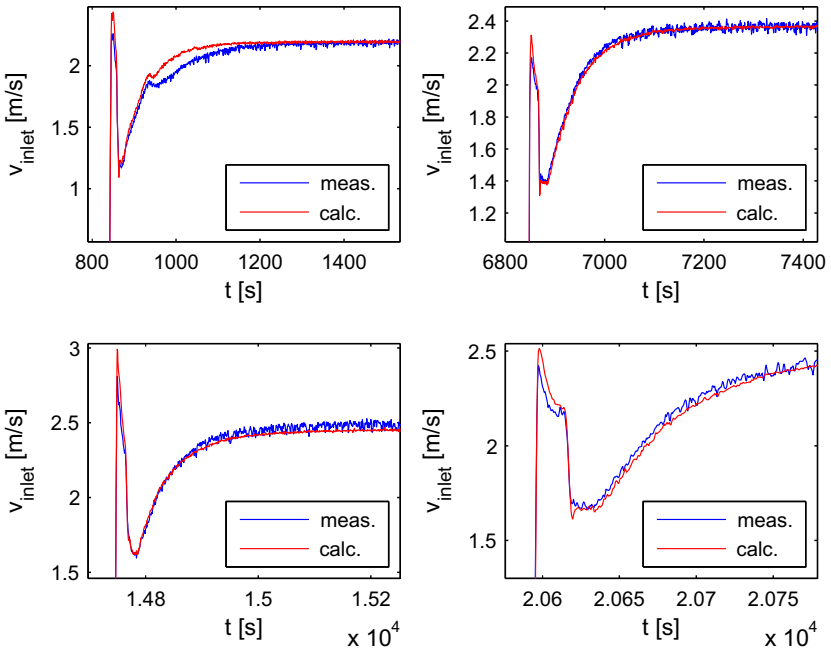

Fig. 7. Details of Fig. 5.

In Figs. 5 and 6 the time courses of the fluid velocities at the inlet and the outlet of the pipeline are shown. Since the velocity measurements are very noisy, only the results of the proposed mutliscale method are shown to improve the legibility of the figure. In Fig. 7 some details of Fig. 5 are depicted, where the transient phases can be seen in detail. Very good agreement between the measured data and the proposed model response can be seen (the model output lies within the measurement noise of the measured signal when the pipeline is not stopped).

6. Conclusion

A model of the pipeline was derived which is suitable for multi-batch driven pipelines. The model is a set of nonlinear partial differential equations and the method of characterisctics is used to transform them into a set of ordinary differential equations defined on different domains. Due to significant difference between the fluid velocity and the speed of sound the resulting model is stiff and a method similar to the multiscale methods for stiff ordinary differential equations was developed. Results of the simulations show that the method is more suitable than the classical one-scale method with respect to numerical diffusion while also being considerably quicker if similar quality of results is wanted. Three integration methods (Euler, exact trapezoidal, approximative trapezoidal) were used to solve the set of ordinary differential equations. The

results of their application on a real problem are practically identical and very close to the measured data, so the conclusion is that any of those methods is suitable for multibatch pipeline simulation.

Appendix A. The derivation of numerical solutions for the trapezoidal method

This appendix includes lengthy formulae for the trapezoidal method given in 4.3.2. Inner points:

$$P(i,k+1)=\frac{\operatorname{sign}(V(i,k))}{\bar{\varphi}^{\lambda}_{RP}+\bar{\varphi}^{\lambda}_{SP}}\left(-\frac{A\bar{\varphi}^{\lambda}_{SP}\Delta t\bar{\varphi}^{\lambda}_{RP}(V(i+\psi,k)-V(i-\xi,k))}{4\Delta t\left(\bar{\varphi}^{\lambda}_{RP}+\bar{\varphi}^{\lambda}_{SP}\right)}+1/4\bar{\varphi}^{\lambda}_{SP}\Delta t\bar{\varphi}^{\lambda}_{RP}\left(V(i+\psi,k)^2+V(i-\xi,k)^2\right)\right.$$
$$\left.+\frac{\sqrt{W}\left(\bar{\varphi}^{\lambda}_{RP}\bar{\varphi}_{SP}-\bar{\varphi}^{\lambda}_{SP}\bar{\varphi}_{RP}\right)}{\Delta t\left(\bar{\varphi}^{\lambda}_{RP}+\bar{\varphi}^{\lambda}_{SP}\right)}\right)+\frac{1}{\bar{\varphi}^{\lambda}_{RP}+\bar{\varphi}^{\lambda}_{SP}}\left(\frac{A\left(\bar{\varphi}^{\lambda}_{RP}\bar{\varphi}_{SP}-\bar{\varphi}^{\lambda}_{SP}\bar{\varphi}_{RP}\right)}{2\Delta t\left(\bar{\varphi}^{\lambda}_{RP}+\bar{\varphi}^{\lambda}_{SP}\right)}+\frac{\sqrt{W}\bar{\varphi}^{\lambda}_{SP}\Delta t\bar{\varphi}^{\lambda}_{RP}(V(i+\psi,k)-V(i-\xi,k))}{2\Delta t\left(\bar{\varphi}^{\lambda}_{RP}+\bar{\varphi}^{\lambda}_{SP}\right)}\right.$$
$$\left.-\bar{\varphi}^{\lambda}_{RP}\bar{\varphi}_{SP}V(i+\psi,k)+\bar{\varphi}^{\lambda}_{SP}P(i-\xi,k)+\bar{\varphi}^{\lambda}_{RP}\Delta t\bar{\varphi}^{\alpha}_{SP}+\bar{\varphi}_{RP}\bar{\varphi}^{\lambda}_{SP}V(i-\xi,k)+\bar{\varphi}^{\lambda}_{RP}P(i+\psi,k)-\bar{\varphi}^{\lambda}_{SP}\Delta t\bar{\varphi}^{\alpha}_{RP}\right),\quad(A.1)$$

$$V(i,k+1)=\frac{1}{\bar{\varphi}^{\lambda}_{RP}+\bar{\varphi}^{\lambda}_{SP}\Delta t}\left(\operatorname{sign}(V(i,k))\left(\sqrt{W}-2\bar{\varphi}_{RP}-2\bar{\varphi}_{SP}\right)-\bar{\varphi}^{\lambda}_{RP}\Delta tV(i-\xi,k)-\bar{\varphi}^{\lambda}_{SP}\Delta tV(i+\psi,k)\right),\quad(A.2)$$

where

$$W=-\bar{\varphi}^{\lambda}_{RP}\bar{\varphi}^{\lambda}_{SP}\Delta t^2(V(i+\psi,k)-V(i-\xi,k))^2+4\left(\bar{\varphi}_{RP}{}^2+\bar{\varphi}^2_{SP}\right)^2+4\operatorname{sign}(V(i,k))\left(\left(\bar{\varphi}^{\lambda}_{RP}\bar{\varphi}_{SP}+\bar{\varphi}^{\lambda}_{SP}\bar{\varphi}_{RP}\right)(V(i-\xi,k)\right.$$
$$+V(i+\psi,k))2\bar{\varphi}_{SP}\bar{\varphi}^{\lambda}_{SP}V(i+\psi,k)+2\bar{\varphi}^{\lambda}_{RP}\bar{\varphi}_{RP}V(i-\xi,k)+\left(\bar{\varphi}^{\lambda}_{RP}+\bar{\varphi}^{\lambda}_{SP}\right)(P(i-\xi,k)-P(i+\psi,k))$$
$$\left.+-\left(\bar{\varphi}^{\lambda}_{RP}+\bar{\varphi}^{\lambda}_{SP}\right)\left(\bar{\varphi}^{\alpha}_{RP}+\bar{\varphi}^{\alpha}_{SP}\right).\right)\Delta t\quad(A.3)$$

and

$$A=-2\Delta t\left(\bar{\varphi}^{\lambda}_{RP}V(i-\xi,k)-\bar{\varphi}^{\lambda}_{SP}V(i+\psi,k)\right),\quad(A.4)$$

Inlet point:

$$W_i=\bar{\varphi}^2_{SP}+\left(2\bar{\varphi}_{SP}\bar{\varphi}^{\lambda}_{SP}\Delta tV(0+\psi,k)+\bar{\varphi}^{\lambda}_{SP}\Delta tP(0,k+1)-\bar{\varphi}^{\lambda}_{SP}\Delta tP(0+\psi,k)-\bar{\varphi}^{\lambda}_{SP}\bar{\varphi}^{\alpha}_{SP}\Delta t^2\right)\operatorname{sign}(V(0+\psi,k)),\quad(A.5)$$

$$V(0,k+1)=-V(i+\psi,k)+\operatorname{sign}(V(0+\psi,k))\frac{-2\bar{\varphi}_{SP}+2\sqrt{W_i}}{\bar{\varphi}^{\lambda}_{SP}\Delta t},\quad(A.6)$$

Outlet point:

$$W_o=\bar{\varphi}^2_{RP}+\left(2\bar{\varphi}^{\lambda}_{RP}\Delta t\bar{\varphi}_{RP}V(N_r-\xi,k)-\bar{\varphi}^{\lambda}_{RP}\Delta tP(N_r,k+1)+\bar{\varphi}^{\lambda}_{RP}\Delta tP(N_r-\xi,k)-\bar{\varphi}^{\lambda}_{RP}\Delta t^2\bar{\varphi}^{\alpha}_{RP}\right)\operatorname{sign}(V(N_r-\xi,k)),\quad(A.7)$$

$$V(N_r,k+1)=-V(N_r-\xi,k)+\operatorname{sign}(V(N_r-\xi,k))\frac{-2\bar{\varphi}_{RP}+2\sqrt{W_o}}{\bar{\varphi}^{\lambda}_{RP}\Delta t}.\quad(A.8)$$

Appendix B. The derivation of numerical solutions for the approximative trapezoidal method

This appendix includes lengthy formulae for the approximative trapezoidal method given in 4.3.3. Inner points:

$$P(i,k+1)=\frac{1}{\bar{\varphi}_{RP}+\bar{\varphi}_{SP}+\bar{\varphi}^{\lambda}_{RP}|V(i-\xi,k)|\Delta t+\bar{\varphi}^{\lambda}_{SP}|V(i+\psi,k)|\Delta t}\times\left(P(i-\xi,k)\bar{\varphi}_{SP}+P(i-\xi,k)\bar{\varphi}^{\lambda}_{SP}|V(i+\psi,k)|\Delta t\right.$$
$$+\bar{\varphi}_{RP}P(i+\psi,k)+\bar{\varphi}_{RP}\bar{\varphi}^{\alpha}_{SP}\Delta t-\bar{\varphi}_{RP}\bar{\varphi}_{SP}V(i+\psi,k)+\bar{\varphi}_{RP}V(i-\xi,k)\bar{\varphi}_{SP}+\bar{\varphi}_{RP}V(i-\xi,k)\bar{\varphi}^{\lambda}_{SP}|V(i+\psi,k)|\Delta t$$
$$-\bar{\varphi}^{\alpha}_{RP}\Delta t\bar{\varphi}_{SP}-\bar{\varphi}^{\alpha}_{RP}\Delta t^2\bar{\varphi}^{\lambda}_{SP}|V(i+\psi,k)|+\bar{\varphi}^{\lambda}_{RP}|V(i-\xi,k)|\Delta tP(i+\psi,k)+\bar{\varphi}^{\lambda}_{RP}|V(i-\xi,k)|\Delta t^2\bar{\varphi}^{\alpha}_{SP}$$
$$\left.-\bar{\varphi}^{\lambda}_{RP}|V(i-\xi,k)|\Delta t\bar{\varphi}_{SP}V(i+\psi,k)\right),\quad(B.1)$$

$$V(i,k+1)=\frac{1}{\bar{\varphi}_{RP}+\bar{\varphi}_{SP}+\bar{\varphi}^{\lambda}_{RP}|V(i-\xi,k)|\Delta t+\bar{\varphi}^{\lambda}_{SP}|V(i+\psi,k)|\Delta t}$$
$$\times\left(P(i-\xi,k)-P(i+\psi,k)+\bar{\varphi}_{RP}V(i-\xi,k)+-\bar{\varphi}^{\alpha}_{RP}\Delta t-\bar{\varphi}^{\alpha}_{SP}\Delta t+\bar{\varphi}_{SP}V(i+\psi,k)\right).\quad(B.2)$$

Inlet point:

$$V(0,k+1)=\frac{P(i,k+1)-P(i+\psi,k)+\bar{\varphi}_{SP}V(i+\psi,k)-\bar{\varphi}^{\alpha}_{SP}\Delta t}{\bar{\varphi}_{SP}+\bar{\varphi}^{\lambda}_{SP}|V(i+\psi,k)|\Delta t},\quad(B.3)$$

Outlet point:

$$V(N_r, k+1) = -\frac{P(i,k+1) - P(i-\xi,k) - \bar{\varphi}_{RP} V(i-\xi,k) + \bar{\varphi}^{\alpha}_{RP}\Delta t}{\bar{\varphi}_{RP} + \bar{\varphi}^{\lambda}_{RP}|V(i-\xi,k)|\Delta t}. \tag{B.4}$$

References

[1] H. Siebert, Untersuchung verschiedener Methoden zur Lecküberwachung bei Pipelines, PhD Thesis, TH Darmstadt, 1981.
[2] L. Billmann, Methoden zur Lecküberwachung und Regelung von Gasfernleitungen, PhD Thesis, TH Darmstadt, 1985.
[3] G. Geiger, W. Gregoritza, D. Matko, Leak detection and localisation in pipes and pipelines, Comput. Aided Chem. Eng. 8 (2000) 781–786.
[4] V.L. Streeter, E.B. Wylie, Fluid Transients, McGraw-Hill, New York, 1978.
[5] D. Matko, G. Geiger, Models of pipelines in transient mode, Math. Comput. Model. Dyn. Syst. 8 (1) (2002) 117–136.
[6] A.H. Shapiro, The Dynamics and Thermodynamics of Compressible Fluid Flow, vol. 1, The Ronald Press Company, 1953.
[7] S. Jang, C. Cho, J. Nam, S.-H. Lim, D. Shin, T.-Y. Chung, Numerical study on leakage detection and location in a simple gas pipeline branch using an array of pressure sensors, Journal of Mechanical Science and Technology 24 (2010) 983–990.
[8] T.J. Chung, Computational Fluid Dynamics, Cambridge University Press, Cambridge, 2002.
[9] J. Kralik, P. Stiegler, Z. Vostry, J. Zavorka, A universal dynamic simulation-model of gas-pipeline networks, IEEE Transactions on Systems Man and Cybernetics 14 (4) (1984) 597–606.
[10] M. Abbaspour, K.S. Chapman, L.A. Glasgow, Transient modeling of non-isothermal, dispersed two-phase flow in natural gas pipelines, Appl. Math. Model. 34 (2) (2010) 495–507.
[11] J.D. Anderson, Basic Philosophy of CFD, in: J.F. Wendt (Ed.), second ed., Computational Fluid Dynamics, Springer-Verlag, Berlin Heidelberg, 1996.
[12] L. Zhang, Y. Guo, S. He, Numerical simulation of three-dimensional incompressible fluid in a box flow passage considering fluid-structure interaction by differential quadrature method, Appl. Math. Model. 31 (9) (2007) 2034–2049.
[13] H.P. Reddy, S. Narasimhan, S.M. Bhallamudi, Simulation and state estimation of transient flow in gas pipeline networks using a transfer function model, Ind. Eng. Chem. Res. 45 (11) (2006) 3853–3863.
[14] A.F. Colombo, P. Lee, B.W. Karney, A selective literature review of transient-based leak detection methods, J. Hydro-Environ. Res. 2 (4) (2009) 212–227.
[15] A. Bergant, A.S. Tijsseling, J.P. Vítkovský, D.I.C. Covas, A.R. Simpson, M.F. Lambert, Parameters affecting water-hammer wave attenuation, shape and timing – Part 1: mathematical tools, J. Hydraul. Res. 46 (3) (2008) 373–381.
[16] S.H. Kim, Extensive development of leak detection algorithm by impulse response method, J. Hydraul. Eng. 131 (3) (2005) 201–208.
[17] J.T. Haskew, M.A.R. Sharif, Performance evaluation of vaned pipe bends in turbulent flow of liquid propellants, Appl. Math. Model. 21 (1) (1997) 48–62.
[18] S. Blažič, D. Matko, G. Geiger, Simple model of a multi-batch driven pipeline, Math. Comput. Simul. 64 (2004) 617–630.
[19] V.L. Streeter, E.B. Wylie, Fluid Mechanics, eighth ed., McGraw-Hill, New York, 1985.
[20] R. Courant, K. Friedrichs, H. Lewy, On the partial difference equations of mathematical physics, IBM J. Res. Dev. 11 (2) (1967) 215–234.
[21] L.N. Trefethen, Finite difference and spectral methods for ordinary and partial differential equations, 1996. <http://people.maths.ox.ac.uk/trefethen/pdetext.html>.
[22] N. Fenichel, Geometric singular perturbation theory for ordinary differential equations, J. Differ. Equ. 31 (1979) 53–98.